J. Earth Planet. Sci. Nagoya Univ., Vol. 41, 45 to 55, 1994

Cotribution of grain-boundary REEs to the chemistry of the glass formed by experimental partial-melting of a quartzose paragneiss

Izumi KAJIZUKA[1], Kazuhiro SUZUKI[1] and Hikari KAMIOKA[2]

Department of Earth and Planetary Sciences, Nagoya University, Nagoya 464-01, Japan[1] and Geological Survey of Japan, Tsukuba 305, Japan[2]
(Received October 3, 1994 / Accepted November 25, 1994)

ABSTRACT

Contribution of grain-boundary REEs (rare earth elements) to the chemistry of the partial melt was examined by in situ melting of a quartzose paragneiss sample. The paragneiss sample, consisting mainly of quartz, oligoclase, biotite and muscovite, contains 24.3ppm La, 53.1ppm Ce, 16.9ppm Nd, 3.91ppm Sm, 0.94ppm Eu, 1.44ppm Yb and 0.23ppm Lu. REE-bearing accessory minerals, 155.9mg zircon, 27.3mg monazite, 13.5mg apatite and 3.1mg xenotime per 1kg sample, account for only 10−15% of the whole-rock abundances. Microprobe investigation reveals that the unaccountable REEs, if not all, reside at grain-boundaries of constituent minerals. The paragneiss produces a partial melt of 40 vol.% through heating at 1350°C and 1 atm for 60 minutes. The melt is andesitic in composition, and contains REEs about twice as much as the whole-rock abundances. The chondrite-normalized REE pattern of the melt is linear and light REE-enriched, a typical pattern for granitoids. Since accessory minerals, at least zircon, monazite and xenotime, remain unmelted, most REEs in the melt must originate from the grain-boundaries. The grain-boundary REEs in source rocks play a key role on the distribution of REEs in granitoids formed through partial melting of crustal rocks.

INTRODUCTION

The geochemistry of REEs, especially the chondrite-normalized REE pattern (Masuda-Coryell diagram), provides a fundamental constraint on the interpretation of the origin and evolution of granitoids. The REE patterns of granitoids are light REE-enriched and linear. They occasionally comprise two linear segments with a turning point around Gd. Most granitoids are currently accepted to be formed through partial melting of crustal rocks (e.g. White and Chappell, 1977). A question, here, arises regarding what mechanism governs the REE abundances and REE patterns of granitoids. Some workers have suggested that the REE abundances are controlled mainly by melting of REE-rich accessory minerals in source rocks (e.g. Watson and Harrison, 1983 and 1984; Harrison and Watson, 1984; Rapp and Watson, 1986). We consider that the linearity of the REE pattern cannot be explained simply by means of

linear combination of REE-rich accessory minerals. Several studies, on the other hand, suggested that REEs in rocks reside mainly at grain-boundaries of constituent minerals (e.g. Masuda, 1969; Suzuki, 1981; Suzuki et al., 1990). If this is the case, the grain-boundary REEs may play a key role on the distribution of REEs in granitoid melts formed through partial melting, because grain-boundaries are the first to melt; the REE pattern of the melts will inherit REE characteristics from the grain-boundaries. This paper reports the contribution of grain-boundary REEs to the melt on the basis of partial melting of a sample of quartzose paragneiss from the Ryoke metamorphic belt, Southwest Japan.

SAMPLE DESCRIPTION

The quartzose paragneiss selected for this study was collected from the Cretaceous Ryoke metamorphic belt, central Japan (Shiidaira, 137°33′17″E, 34°57′50″N). It occurs as an interstratified lens of about 60cm in thickness within alternations of pelitic and psammitic gneisses metamorphosed under the condition of the andalusite-sillimanite transition. The gneiss specimen consists mainly of quartz (67.0%), oligoclase (24.0%), biotite (6.8%) and muscovite (2.2%). We selected this sample because it contains large quantity of equigranular quartz. That is, as mentioned later, melt derived by partial melting of this gneiss could be observed clearly at quartz grain boundaries. Quartz grains are irregular to subrounded in shape and about 0.5mm in diameter. Oligoclase (An_{23-30}) occupies interstitial regions between quartz grains. Biotite and muscovite occur as flakes of 0.05—0.1mm in length. Some biotite flakes alter into chlorite along their cleavages.

Accessory minerals are zircon, monazite, apatite, xenotime, pyrite, pyrrhotite, ilmenite and rutile. Most zircon grains occur as faceted euhedral prisms of 0.1—0.2mm in length, however, some are well rounded. Monazite forms subhedral to anhedral grains of 0.06—0.15mm in size. Apatite, about 0.1mm in size, is anhedral, and xenotime forms anhedral grains of 0.1—0.3mm in size.

In order to determine the amount of accessory minerals present as precisely as possible, we separate heavy minerals (density > 3.0 g/cm^3) from a chip of 718.3g following the procedure described by Suzuki et al. (1990). After removing pyrrhotite with a magnet, and biotite, ilmenite and light minerals with an isodynamic magnetic separator and a heavy liquid, the heavy minerals, zircon, monazite, apatite, xenotime, pyrite and rutile, amount to 337.7mg. They were mounted on a glass slide with an epoxy resin, polished and analyzed modally on an electron microprobe; each accessory mineral was irradiated electron beam and could be distinguished by characteristic X-rays. The analysis enables us to calculate the amount of each accessory mineral per 1 kg sample: 155.9mg zircon, 27.3mg monazite, 13.5mg apatite, 3.1mg xenotime, 270.0mg pyrite and a trace amount of rutile. The modal composition was checked by means of point counts coupled with microprobe identification of minerals over a large surface area and a large number of points (19,038 points were counted over 10 thin sections). This alternative analysis shows

about 0.01 vol.% zircon, namely ca. 170mg zircon per 1 kg. Since both analyses give nearly identical results with respect to the amounts of zircon and monazite, we believe that the mode is accurate with an uncertainty of ±10%.

REEs IN ACCESSORY MINERALS AND GRAIN-BOUNDARIES

The REE contents of the accessory minerals were determined on a JXA-5A electron microprobe. The operating conditions were 15 kV accelerating voltage, about 5 μm beam diameter, 0.01—0.1 μA beam current and 40—200 sec. counting time. The measurement of X-ray intensity for the line peak and background was repeated twice or three times, and the arithmetic average was taken. Details of the analytical procedure including correction of spectral interferences are discussed in Suzuki et al. (1990). The detection limits at the 2σ confidence level are 0.01 wt.% for most REE oxides, and the relative error in the determination is about 10% on the 0.1 wt.% level and less than 5% on the 1 wt.% level. Representative microprobe analyses of individual accessory minerals are listed in Table 1.

Table 1. Selected electron microprobe analyses (wt.%) of accessory minerals in the quartzose paragneiss from the Shitara area of the Ryoke metamorphic belt, central Japan.

	Zircon				Apatite	
SiO_2	32.8	32.9	32.7	Sm_2O_3	0.020	0.017
ZrO_2	64.8	64.9	64.5	Gd_2O_3	0.057	0.054
HfO_2	1.60	1.28	1.98	Dy_2O_3	0.081	0.063
Y_2O_3	0.117	0.345	0.210	Er_2O_3	0.028	0.025
Dy_2O_3	-	0.026	-	CaO	55.0	55.3
Er_2O_3	0.015	0.051	0.023	P_2O_5	42.10	42.1
Yb_2O_3	0.026	0.081	0.045	F	3.66	3.65
P_2O_5	0.100	0.098	0.195			
Total	99.4_{58}	99.6_{81}	99.6_{53}	Total	100.9_{46}	101.2_{09}

	Monazite					Xenotime
SiO_2	-	0.119	2.02	2.92	0.669	0.100
ThO_2	4.97	4.63	12.1	18.2	9.61	-
UO_2	0.210	0.150	0.626	0.686	1.29	0.509
Y_2O_3	2.91	1.00	0.905	1.30	1.16	43.4
La_2O_3	14.9	16.5	11.5	10.1	7.87	0.011
Ce_2O_3	26.8	29.5	26.0	24.0	26.0	0.113
Pr_2O_3	2.76	2.80	2.88	2.72	3.02	-
Nd_2O_3	11.0	10.6	12.1	10.1	13.3	0.438
Sm_2O_3	1.34	1.72	2.39	1.94	2.96	0.492
Gd_2O_3	1.43	0.966	0.815	0.966	1.26	1.78
Tb_2O_3	0.171	0.053	0.042	0.169	0.209	0.542
Dy_2O_3	0.797	0.273	0.253	0.294	0.322	5.15
Ho_2O_3	-	-	-	0.061	0.056	1.48
Er_2O_3	-	-	-	-	-	4.47
Tm_2O_3	-	-	-	-	-	0.809
Yb_2O_3	-	-	-	-	-	4.39
Lu_2O_3	-	-	-	-	-	0.549
PbO	0.089	0.021	0.056	0.201	0.930	-
CaO	1.15	0.854	0.700	0.821	1.64	-
P_2O_5	30.9	30.2	27.0	25.4	28.9	35.1
Total	99.4_{27}	99.3_{86}	99.3_{87}	99.8_{78}	99.1_{96}	99.3_{33}

Zircon contains small amounts of Y and heavy REEs, whereas light REEs such as La, Ce and Nd can not be usually detected on the electron microprobe. Figure 1A illustrates the frequency distribution of the Yb_2O_3 content in 62 zircon grains. The Yb_2O_3 contents range from 0.01 to 0.17 wt.%, and concentrate at around 0.07 wt.%. The arithmetic average of zircon analyses gives 0.020 ± 0.009 wt.% Dy_2O_3, 0.036 ± 0.050 Er_2O_3 and 0.075 ± 0.047 Yb_2O_3. The chondrite-normalized REE pattern shows heavy REE-enrichment with a normalized Dy/Yb ratio of 0.17 (Fig. 2).

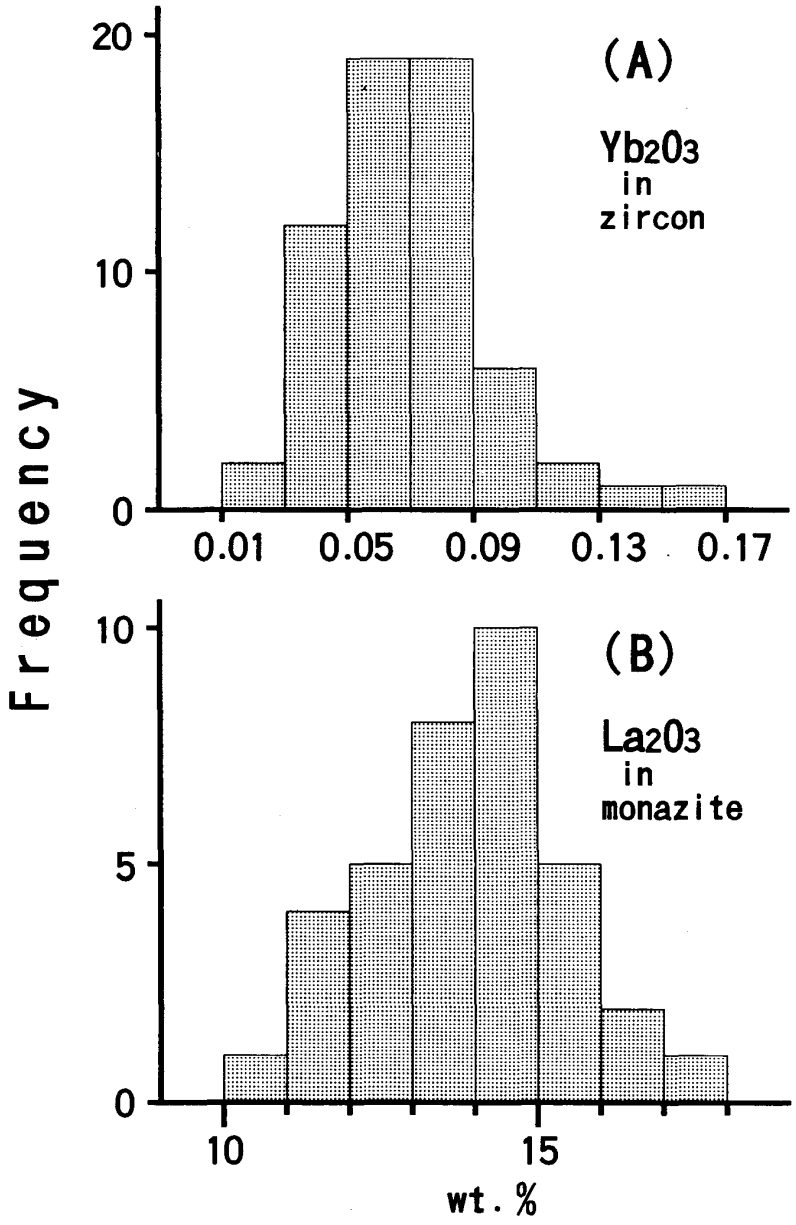

Fig. 1. Frequency distribution diagrams for the Yb_2O_3 content of 62 zircon grains (A) and for the La_2O_3 content of 36 monazite grains (B) in the quartzose paragneiss from the Ryoke metamorphic belt.

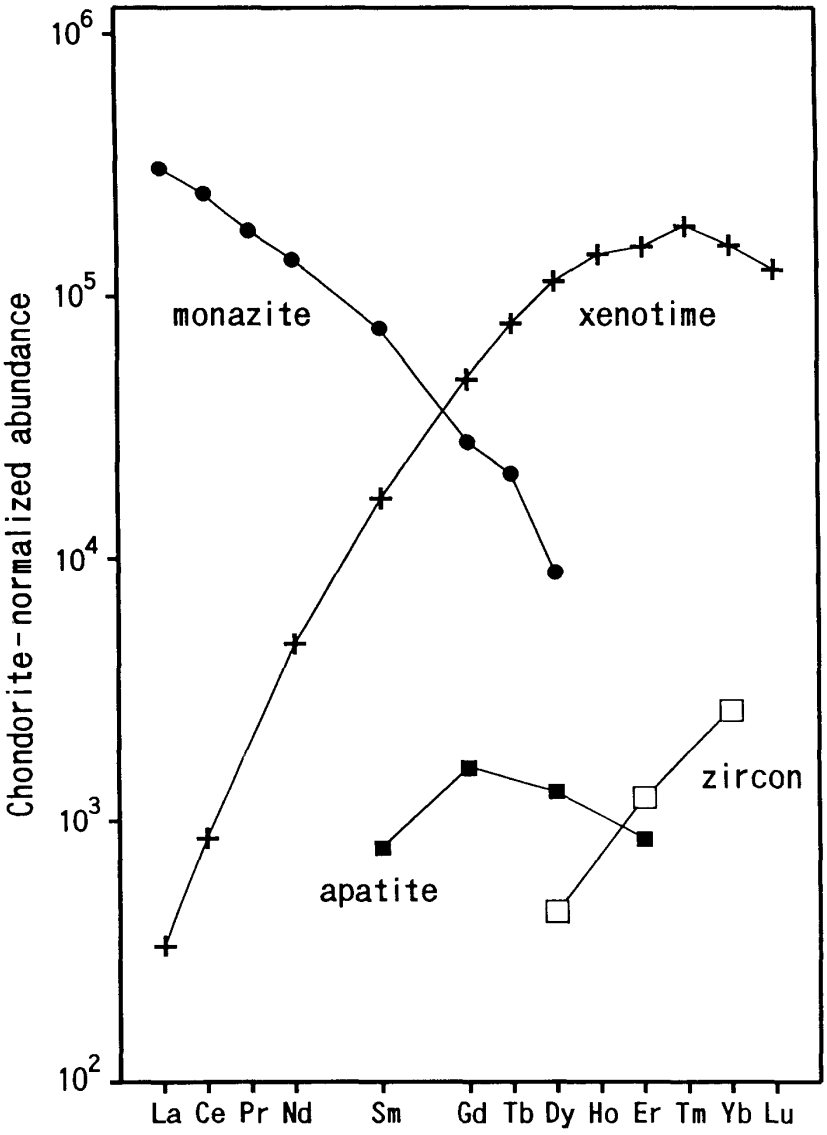

Fig. 2. Chondrite-normalized patterns for the average REE abundances of zircon, monazite, apatite and xenotime in the quartzose paragneiss. Chondrite abundances are after Masuda et al. (1973) and Masuda (1975).

Monazite contains 4.4—12.1 wt.% ThO_2 and 0.05—1.3 wt.% UO_2. Compositional variation of monazite is mainly due to the different concentration of ThO_2 and UO_2; the relative abundance among REEs does not change significantly from grain to grain as well as within individual grains. The frequency distribution of the La_2O_3 content in 36 monazite grains is illustrated in Fig. 1B. Monazite analyses average 13.6 ± 1.8 wt.% La_2O_3, 27.9 ± 1.4 Ce_2O_3, 2.82 ± 0.23 Pr_2O_3, 11.5 ± 0.9 Nd_2O_3, 2.02 ± 0.32 Sm_2O_3, 0.992 ± 0.254 Gd_2O_3, 0.143 ± 0.060 Tb_2O_3 and 0.396 ± 0.175 Dy_2O_3. The REE pattern shows a sharp decrease toward the heavy REE end (Fig. 2).

Apatite is fluorapatite with ca. 3.6% F, and contains 0.021 ± 0.002 wt.% Sm_2O_3, 0.057 ± 0.003 Gd_2O_3, 0.058 ± 0.025 Dy_2O_3 and 0.025 ± 0.002 Er_2O_3. The REE

pattern is a convex with a broad maximum around Gd (Fig. 2).

Xenotime concentrates middle to heavy REEs with average 0.015 ± 0.004 wt.% La_2O_3, 0.098 ± 0.015 Ce_2O_3, 0.400 ± 0.038 Nd_2O_3, 0.458 ± 0.033 Sm_2O_3, 1.74 ± 0.04 Gd_2O_3, 0.538 ± 0.014 Tb_2O_3, 5.08 ± 0.07 Dy_2O_3, 1.47 ± 0.01 Ho_2O_3, 4.50 ± 0.03 Er_2O_3, 0.809 ± 0.05 Tm_2O_3, 4.43 ± 0.04 Yb_2O_3 and 0.564 ± 0.014 Lu_2O_3. The REE pattern is a convex with a broad maximum around Tm (Fig. 2).

We now consider the fraction of REE contained in the accessory minerals on the basis of the average REE contents and the mode. On the electron microprobe, La, Ce and Nd are detected only from monazite and xenotime. The weighted sum of monazite and xenotime provides 3.2ppm La, 6.5 Ce and 2.7 Nd; the two minerals share 13, 12 and 16% of the whole-rock La, Ce and Nd, respectively. Sm is detected from monazite, apatite and xenotime; the weighted sum of these minerals provides 0.49ppm Sm which corresponds to 13% of the whole-rock abundance. Zircon and xenotime provide 0.23ppm Yb, i.e. 16% of the whole-rock Yb. Lu contained in xenotime amounts to 0.02ppm, about 8% of the whole-rock Lu.

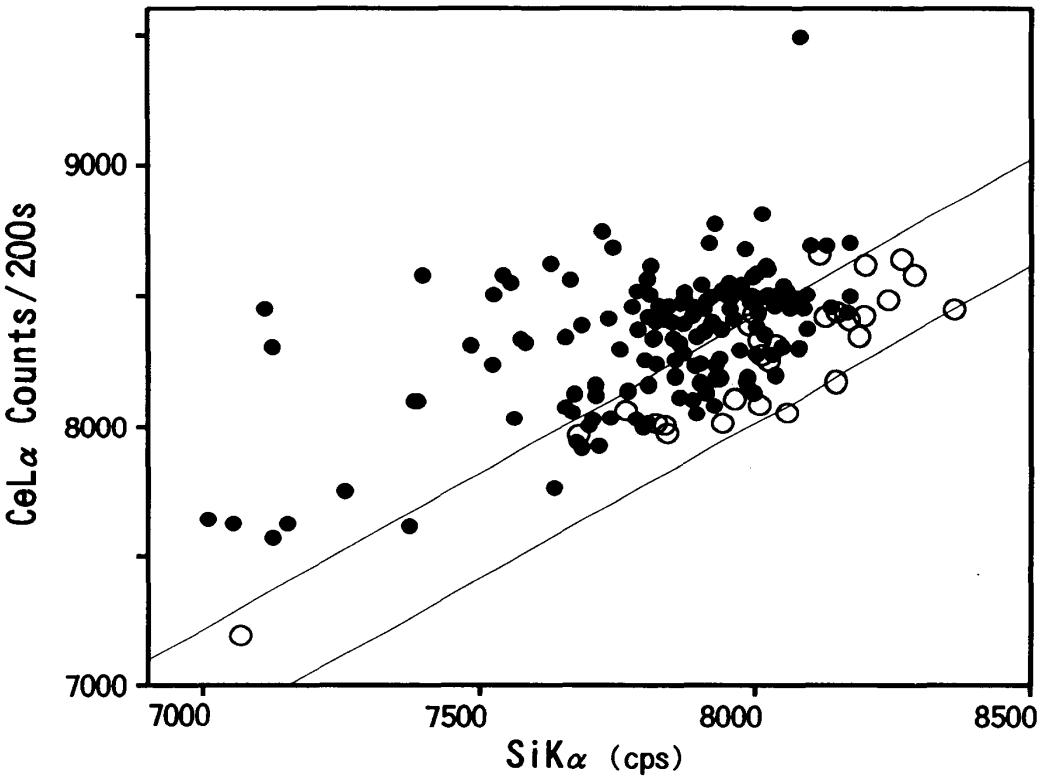

Fig. 3. X-ray counts at CeLα detection position vs. SiKα for grain-boundaries between quartz grains (solid circle) and for interiors of quartz grains (open circle) measured on the electron microprobe. The variation in SiKα counts for interiors of quartz grains is due to the drift of beam current during a long span of the experimental run. The X-ray counts at CeLα detection position for grain-boundaries are higher than those for interiors of quartz grains (e.g. backgrounds), suggesting concentration of Ce at grain-boundaries.

The unaccountable REEs (whole-rock minus sum of accessories) amount to 21.1ppm La, 46.6 Ce, 14.2 Nd, 3.42 Sm, 1.21 Yb and 0.21 Lu, about 85—90% of the whole-rock REEs. Because the main constituent minerals, quartz, oligoclase, biotite and muscovite, contain little REEs (e.g. Fourcade and Allegre, 1981; Gromet and Silver, 1983; Mittlefehldt and Miller, 1983), most of the unaccountable REEs are considered to reside at grain-boundaries of the constituent minerals. To test the grain-boundary enrichment of REEs, we measured X-ray intensities at CeLα-detection position on interiors of quartz grains and boundaries between quartz grains (Fig. 3). X-ray counts (background plus CeLα and possible BaLβ lines) for the grain-boundaries are systematically higher than those for the interiors of quartz grains, suggesting considerable concentration of Ce at the grain-boundaries. The grain-boundary concentration of Ce is neither due to an increase in the Ce content in the lattice of quartz nor to the presence of minute crystalline phases. We believe that the grain-boundary Ce forms a thin surface film.

CONTRIBUTION OF THE GRAIN-BOUNDARY REEs TO THE PARTIAL MELTING PRODUCT

The grain-boundary concentration of REEs suggests that partial melting product enriched in REEs can be formed through in situ melting at grain-boundaries without any contribution of REE-rich accessory minerals. To evaluate this possibility chips (15×15×5mm) of the gneiss were heated at 1 atm in an electric furnace. The temperature was 1350°C, and the heating duration was 60 min. Quenching was done by dipping the sample into distilled water. The heating was conducted three times. After each run, the chip was halved lengthwise and repeatedly washed with distilled water. One half was impregnated with an epoxy resin, ground and prepared as a polished thin section for the microscope observation and microprobe analysis. The other half was crushed with an agate mortar only to the extent necessary for isolation of glass particle from unmelted minerals and preserved for separation of glass.

Oligoclase, biotite and muscovite disappeared by heating, and a 40 vol.% glass (melting product) was formed among quartz grains throughout all heating runs. Since quartz grains became well rounded, they were partly molten. Of accessory minerals, zircon, monazite and xenotime were recognized in the quenched glass of the experimental products, but apatite was not, despite its initial concentration. Although the modal analysis of these accessory minerals was never feasible owing to the small counting area, we consider that most zircon, monazite and xenotime grains, if not all, remain unmelted. Preservation of well-faceted euhedral zircons supports this interpretation.

The major elements of the quenched glass were analyzed on the electron microprobe with 15 kV accelerating voltage, 0.0125 μA beam current and 10 μm beam diameter. The glass is homogeneous in composition throughout individual experimental charges, and the composition is reproducible in all experiments at 1350°C. The average composition is compared in Table 2 with

Table 2. Wet chemical and instrumental neutron activation (INA) analyses of the quartzose paragneiss and the glass formed through partial melting at 1350°C and 1 atm.

Major elements (wt.%)	Gneiss	Glass
SiO_2	83.62	61.4
TiO_2	0.26	0.38
Al_2O_3	9.58	22.9
Fe as FeO	1.18	3.02
MnO	0.03	-
MgO	0.37	1.10
CaO	1.30	3.02
Na_2O	2.38	5.30
K_2O	0.30	1.16
P_2O_5	0.01	-
Ig. loss	0.72	-
$H_2O(-)$	0.09	-
Total	99.84	98.28

REEs (ppm)	INA *	INA *	Calc. **
La	24.3 ±0.1	54.7 ±0.3	53
Ce	53.1 ±1.8	109.9 ±0.6	120
Nd	16.9 ±4.6	45.3 ±3.7	36
Sm	3.91±0.02	8.17±0.02	8.6
Eu	0.94±0.12	1.37±0.06	-
Tb	-	1.15±0.19	-
Yb	1.44±0.08	2.14±0.04	3.0
Lu	0.23±0.02	0.33±0.01	0.5

*Uncertainties due solely to γ-ray counting errors in 1σ.
**See text.

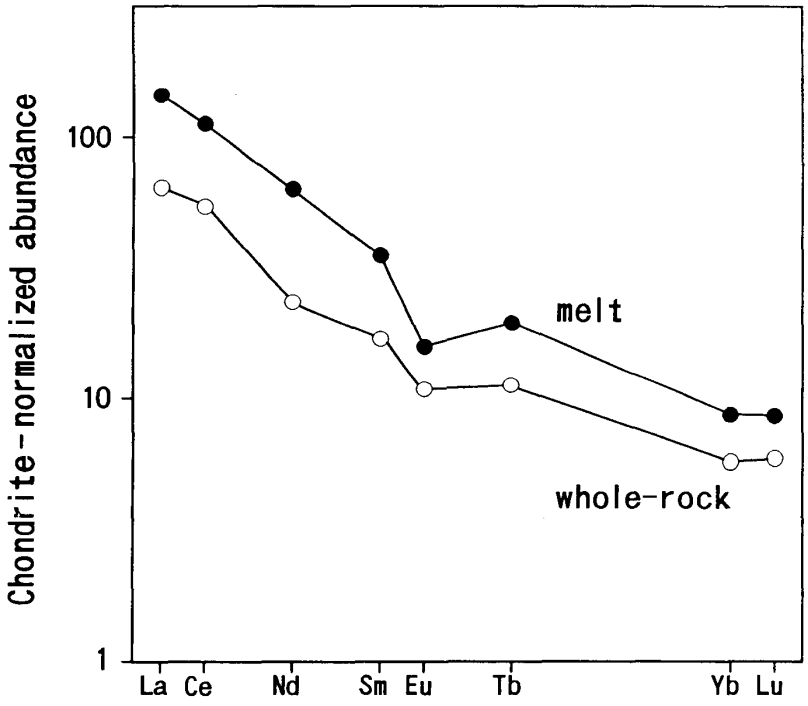

Fig. 4. Chondrite-normalized REE patterns of the quartzose paragneiss and glass formed through 40% partial melting.

the whole-rock composition of the gneiss, determined with a wet chemical method including gravimetry, EDTA titration, colorimetry and atomic absorption photometry. The glass composition clearly differs from the whole-rock composition of the gneiss and also from the ideal compositions of oligoclase. It is andesitic in composition and is characterized by a high proportion of normative corundum, about 7.5%.

The glass was hand-picked from the crushed samples and analyzed for REEs by the instrumental neutron activation analysis method. The details of analytical procedure is described in Tanaka et al. (1988). The result is given in Table 2 together with the whole-rock REE abundance of the gneiss, and the REE pattern is illustrated in Fig. 4. The glass contains REEs about twice as much as the whole-rock abundances. Since REE-rich zircon, monazite and xenotime, as described above, remain unmelted, REEs in the glass are interpreted to have originated from the grain-boundaries.

In the light of the result of our study, we now consider the balance of REEs between the grain-boundaries and the glass. The grain-boundary La (the whole-rock abundance minus the weighted sum of accessories), for example, amounts to 87% of the whole-rock abundance. This provides about 53ppm La in the melt formed by 40% melting (approximately 40 vol.% = 40 wt.%) of the gneiss without any contribution of REE-rich accessory minerals. This calculated La abundance is in good agreement with the observed abundance of 54.7ppm in the glass. The same calculation was carried out for other REEs, and the result is listed in Table 2. The overall consistency between the calculated and observed abundances confirms the view that REEs in the partial melt may originate mainly from grain-boundaries.

The chondrite-normalized REE pattern of the glass is logarithmically linear with a negative Eu-anomaly and a normalized La/Lu ratio of about 10 (Fig. 4). Strictly speaking, the REE pattern is composed of two linear segments with turning point around Gd. This type of REE pattern has been recognized from many granitoids (see discussion in Suzuki et al., 1990). Partitioning of REEs between REE-rich accessory minerals and melts can not explain the linearity and the break, because the partition coefficients for any minerals give a parabola-shape or a part of parabola-shape with no substantial discontinuity: modeling of REE behavior based on mineral phases alone, a common practice in the past, is not valid. We emphasize that the REE characteristics of granitoids formed by partial melting are governed essentially by the grain-boundary REEs in source rocks.

CONCLUSION

(1) The quartzose paragneiss from the Ryoke metamorphic belt in Southwest Japan contains 155.9mg zircon, 27.3mg monazite, 13.5mg apatite and 3.1mg xenotime per 1 kg. The sum of REEs of these accessory minerals accounts for only about 15% of the whole-rock REEs. The rest of REEs are considered to reside at grain-boundaries of the constituent minerals, possibly

forming a surface film.

(2) The gneiss yields a 40 vol.% glass of andesitic composition among quartz grains through heating at 1350°C and 1 atm for 60 minutes. Although most REE-bearing accessory minerals remain unmelted, the quenched glass is concentrated in REEs twice as much as the gneiss abundance, suggesting the derivation of REEs from the grain-boundaries.

ACKNOWLEDGEMENTS

We thank Drs. K. Shibata, T. Tanaka, M. Adachi and M. Enami of Nagoya University for valuable discussion. Instrumental neutron activation analyses were made at the Geological Survey of Japan. This work was supported in part by Grant-in-Aid for fundamental Scientific Research (Nos. 04402016 and 04-1634) from the Ministry of Education, Science and Culture, Japan. IK acknowledges the receipt of JSPS Fellowships for Japanese Junior Scientists.

REFERENCES

Fourcade, S. and Allegre, C.J. (1981) Trace elements behavior in granite genesis: A case study the calc-alkaline plutonic association from Querigut complex (Pyrénées, France). *Contrib. Mineral. Petrol.* **76**, 177–195.

Gromet, L.P. and Silver, L.T. (1983) Rare earth element distributions among minerals in a granodiorite and their petrogenetic implications. *Geochim. Cosmochim. Acta*, **47**, 925–939.

Harrison, T.M. and Watson, E.B. (1984) The behavior of apatite during crustal anatexis: Equilibrium and kinetic considerations. *Geochim. Cosmochim. Acta*, **48**, 1467–1477.

Masuda, A. (1969) Genesis of basalts viewed from a model, assuming solidification of original melt with chondritic lanthanides, with particular reference to apparent uniform enrichment factors. *Geochem. J.* **3**, 153–160.

Masuda, A. (1975) Abundances of monoisotopic REE, consistent with the Leedy chondrite values. *Geochem. J.* **9**, 183–184.

Masuda, A., Nakamura, N. and Tanaka, T. (1973) Fine structures of mutually normalized rare-earth patterns of chondrites. *Geochim. Cosmochim. Acta*, **37**, 239–248.

Mittlefehldt, D.W. and Miller, C.F. (1983) Geochemistry of the Sweetwater Wash Pluton, California: Implications for "anomalous" trace element behavior during differentiation of felsic magmas. *Geochim. Cosmochim. Acta*, **47**, 109–124.

Rapp, R.P. and Watson, E.B. (1986) Monazite solubility and dissolution kinetics: implications for the thorium and light rare earth chemistry of felsic magmas. *Contrib. Mineral. Petrol.* **94**, 304–316.

Suzuki, K. (1981) Grain boundary concentration of rare earth elements in a hornblende cumulate. *Geochem. J.* **15**, 295–303.

Suzuki, K., Adachi, M. and Yamamoto, K. (1990) Possible effects of grain-boundary REE on the REE distribution in felsic melts derived by partial melting. *Geochem. J.* **24**, 57–74.

Suzuki, K. and Adachi, M. (1991) Precambrian provenance and Silurian metamorphism of the Tsubonosawa paragneiss in the South Kitakami terrane, Northeast Japan, revealed by the chemical Th-U-total Pb isochron ages of monazite, zircon and xenotime. *Geochem. J.* **25**, 357–376.

Tanaka, T., Kamioka, H. and Yamanaka, K. (1988) A fully automated γ-ray counting and data processing system for INAA and analysis of rock reference samples. *Bull. Geol. Surv. Japan*, **39**, 537–557.

Watson, E.B. and Harrison, T.M. (1983) Zircon saturation revisited: temperature and composition effects in a variety of crustal magma types. *Earth Planet. Sci. Lett.* **64**, 295–304.

Watson, E.B. and Harrison, T.M. (1984) Accessory minerals and the geochemical evolution of crustal magmatic systems: a summary and prospectus of experimental approaches. *Phys. Earth Planet. Int.* **35**, 19–30.

White, A.J.R. and Chappell, B.W. (1977) Ultrametamorphism and granitoid genesis. *Tectonophysics*, **43**, 7–22.